# *Articles*

## Control of Particle Size and Surface Properties of Crystals of NaX Zeolite

Bi-Zeng Zhan,[†] Mary Anne White,*[,†] Michael Lumsden,[†] Jason Mueller-Neuhaus,[‡] Katherine N. Robertson,[†] T. Stanley Cameron,[†] and Michael Gharghouri[§]

*Department of Chemistry, Dalhousie University, Halifax, Nova Scotia B3H 4J3, Canada, Department of Physics, Dalhousie University, Halifax, Nova Scotia B3H 3J5, Canada, and Department of Mining and Metallurgical Engineering, Dalhousie University, Halifax, Nova Scotia B3J 2X4, Canada*

*Received December 12, 2001. Revised Manuscript Received March 27, 2002*

We have successfully synthesized NaX zeolite crystals with controlled sizes from 20 nm to 0.8 $\mu$m, using a novel organic-additive-free approach. We show that the NaX crystal size depends on the silicate source and hydrothermal crystallization conditions, especially crystallization temperature and agitation. The physical properties of NaX-nano (20−100 nm) were characterized by X-ray diffraction, high-resolution scanning electron microscopy, FT-IR spectroscopy, $^{29}$Si solid-state NMR spectroscopy, and $N_2$ adsorption. The results were compared with those for micrometer-sized NaX crystals, NaX-$\mu$. As expected, the external surface area of NaX-nano was found to be significantly enhanced compared with that of NaX-$\mu$. Porosity analysis indicates that NaX-nano has a broad distribution of mesopores from 2 to 20 nm, associated with interparticle voids. Both FT-IR and $^{29}$Si solid-state NMR spectra revealed the presence of $Q^3$ silicon atoms in NaX-nano. All four $Q^3$ species were assigned in the $^{29}$Si NMR spectra.

### Introduction

The synthesis of nanometer-dimension zeolites has received much attention in the past decade because nanometer-sized zeolitic crystals can have different properties than their micrometer-sized counterparts.[1−10] The reduction of the particle size from the micrometer to the nanometer scale can change the mass- and heat-transfer resistances in catalytic and sorption processes, thereby improving the catalytic selectivity and reducing coke formation in some petroleum reactions.[11] Furthermore, nanocrystalline zeolites can be used to fabricate zeolitic membranes and ordered porous materials.[12−15] Various nanometer-sized zeolites, including NaA, faujasite-X and -Y, ZSM-5, and silicate-1, can be synthesized via hydrothermal procedures using clear aluminosilicate solutions in the presence of organic templates.[1−10] For instance, nanocrystalline faujasite zeolites have been synthesized with the assistance of tetramethylammonium (TMA) as a template.[1−3,6] However, the organic-template approach has several drawbacks. These templates are expensive and nonrecyclable, and the removal of the templates can lead to an irreversible aggregation of nanocrystals into larger solid particles.[16] We are interested in the synthesis of nanometer-sized zeolites, in part because they are the most widely used catalysts in petroleum cracking and reforming processes.[17] In an earlier communication, we re-

* To whom correspondence should be addressed. E-mail: Mary.Anne.White@DAL.ca. Tel.: +902-494-3894. Fax: +902-494-3894.
† Department of Chemistry.
‡ Department of Physics.
§ Department of Mining and Metallurgical Engineering.

(1) Schoeman, B. J.; Sterte, J.; Otterstedt, J.-E. *Zeolites* **1994**, *14*, 110.
(2) Castagnola, N. B.; Dutta, P. K. *J. Phys. Chem. B* **1998**, *102*, 1696.
(3) Zhu, G.; Qiu, S.; Yu, J.; Sakamoto, Y.; Xiao, F.; Xu, R.; Terasaki, O. *Chem. Mater.* **1998**, *10*, 1483.
(4) Bo, W.; Hongzhu, M. *Microporous Mesoporous Mater.* **1998**, *25*, 131.
(5) Ravishankar, R.; Kirschhock, C.; Schoeman, B. J.; Vanoppen, P.; Grobet, P. J.; Storck, S.; Maier, W. F.; Martens, J. A.; De Schryver, F. C.; Jacobs, P. A. *J. Phys. Chem. B* **1998**, *102*, 2633.
(6) Mintova, S.;Valtchev, V. *Stud. Surf. Sci. Catal.* **1999**, *125*, 141.
(7) Madsen, C.; Jacobsen, C. J. H. *Chem. Commun.* **1999**, 673.
(8) Mintova, S.; Olson, N. H.; Valtchev, V.; Bein, T. *Science* **1999**, *283*, 958.
(9) Xu, M.; Cheng, M.; Bao, X. *Chem. Commun.* **2000**, 1873.
(10) Lassinantti, M.; Hedlund, J.; Sterte, J. *Microporous Mesoporous Mater.* **2000**, *38*, 25.
(11) *Method of Analysis for Fluid Cracking Catalysts*; Grace and Co., Davison Chemicals: Baltimore, MD, 1980.
(12) Huang, L.; Wang, Z.; Sun, J.; Miao, L.; Li, Q.; Yan, Y.; Zhao, D. *J. Am. Chem. Soc.* **2000**, *122*, 3530.
(13) Wang, X. D.; Yang, W. L.; Tang, Y.; Wang, Y. J.; Fu, S. K.; Gao, Z. *Chem. Commun.* **2000**, 2161.
(14) Boudreau, L. C.; Kuck, J. A.; Tsapatsis, M. *J. Membr. Sci.* **1999**, *152*, 41.
(15) Cho, G.; Lee, J.-S.; Glatzhofer, D. T.; Fung, B. M.; Yuan, W. L.; O'Rear, E. A. *Adv. Mater.* **1999**, *11*, 497.
(16) Wang, H.; Wang, Z.; Yan, Y. *Chem. Commun.* **2000**, 2333.

10.1021/cm011635f CCC: $22.00 
Published on Web 06/22/2002

ported our novel and organic-additive-free method to synthesize nanocrystalline NaX zeolite (NaX-nano).[18] This approach has the following advantages: (a) It is possible to control the size of the crystals. (b) It is more efficient and economical than processes using organic templates. (c) It advances our understanding of nucleation and crystal growth during the hydrothermal process. (Kasahara et al.[19] found that ultrafine faujasite crystals formed from a clear aqueous nuclei solution in the very early aging stage effectively produce zeolite-Y.) (d) With this approach, it is possible to synthesize the zeolitic host matrix directly around guest molecules, making nanocomposites by the "build-the-bottle-around-the-ship" method.[20,21] This one-step method offers several other advantages for the synthesis of nanocomposites, including high purity and homogeneity.

Here, we report more detailed studies of synthetic conditions used to control the particle size of NaX crystals and characterization of the resulting materials. In comparison with micrometer-sized NaX (referred to as NaX-$\mu$), several novel properties of NaX-nano are revealed by FT-IR spectroscopy, $N_2$ absorption, and $^{29}$Si solid-state NMR spectroscopy.

## Experimental Methods

**Preparation of Samples.** The chemical reagents used included fumed silica (11 nm, Sigma), tetraethyl orthosilicate (TEOS, Aldrich), SM-30 colloidal silica (Aldrich), silica (20−40 $\mu$m, Aldrich), NaOH (Aldrich), $Al(OH)_3$ (McArthur Chemical), and $NaAlO_2$ (Allied Chemical). All were used without further purification.

Molecular sieve 13X with an average particle size of 2 $\mu$m was purchased from Aldrich. It was calcined in air at 500 °C for 4 h to remove any organic residues before being used further. The calcined sample is referred to hereafter as NaX-Ald.

The nanometer-sized faujasite-X zeolite was synthesized by hydrothermal crystallization in a temperature-controlled shaker. Aluminosilicate gel was prepared by mixing freshly prepared aluminate and silicate solutions together in the molar ratio 5.5 $Na_2O$:1.0 $Al_2O_3$:4.0 $SiO_2$:190 $H_2O$. Typically, an aluminosilicate gel containing 5.34 g of NaOH, 2.42 g of $NaAlO_2$, 3.43 g of $SiO_2$, and 50.0 g of $H_2O$ was adopted. SM-30, fumed silica, and TEOS were chosen as the silicate sources. For TEOS, the hydrolysis was controlled at 0 °C to obtain nanometer-sized aluminosilicate gel. First, a 250-mL plastic bottle containing freshly prepared sodium aluminate solution and a stirring bar was immersed into an ice−water bath. The mixture was cooled for 1 h with stirring. Next, a measured amount of TEOS was added. Stirring was continued at 0 °C for 6 h and then at room temperature for another 24 h. For SM-30 and fumed silica, the silicate sources were directly mixed with freshly prepared aluminate solution at room temperature and then immediately moved to a shaker at the desired temperature for hydrothermal crystallization. Hydrothermal crystallization was conducted at 60 °C for 1−4 days in a shaker with a rotation rate of 250 rpm. The powdered products were recovered with centrifugation, washed with DI water until pH < 8, and then dried at room temperature for 24 h for further characterization. X-ray fluorescence analysis shows that the Si/Al ratio for the 4-day crystallization sample was 1.25, within the range of 1.0−1.5 for NaX. Hereafter, this sample is referred to as NaX-nano, based on the characterization results described below.

To investigate the effect of the synthetic conditions on the final crystal sizes of NaX, other experiments were carried out using all of the same conditions as for the synthesis of NaX-nano, but with fumed silica as the silicate source. In these experiments, the effects of temperature, agitation (stirring/shaking), and duration of the crystallization were investigated. Again, the powdered products were completely washed with DI water until pH < 8 and then dried at room temperature for 24 h before further characterization. Within the range of crystallization parameters investigated (temperatures up to 90 °C, no agitation to 250 rpm shaking, 1−4 days for crystallization), X-ray fluorescence analysis showed that the Si/Al ratio was 1.25 ± 0.05, again within the range of 1.0−1.5 for NaX, although other properties varied somewhat. For example, hydrothermal crystallization at 90 °C for 2 days with no agitation produced particles of larger sizes, hereafter denoted NaX-$\mu$ (see below for details). Because of the limited temperature range of the shaker, all high-temperature syntheses, e.g., 90 °C, were performed in an oil bath with the stirring rate and temperature controlled by a hotplate.

**Characterization.** X-ray powder diffraction (XRD) patterns were recorded at 20 °C on a Rigaku Miniflex system using Cu K$\alpha$ radiation (30 kV, 15 mA ) with a scanning speed of 1° ($2\theta$) min$^{-1}$. The crystallinity of each sample was determined from the peak areas of 6° [111], 16° [331], and 27° [642] using NaX-Ald as a reference.

High-resolution scanning electron microscopy (HRSEM) images were obtained on uncoated samples with a Hitachi S4700 cold-field emission scanning electron microscope operated at 3 keV. Micrometer-sized crystals were imaged using a JEOL 35CF SEM with a 10-kV accelerating voltage.

FT-IR spectra were recorded on a Nicolet 510P FT-IR spectrometer with 4 cm$^{-1}$ resolution. The zeolite powders were mixed with Nujol and then dispersed on a CsI pellet. In each case, 32 scans were used.

Solid-state single-pulse/magic-angle-spinning (SP/MAS) and $^1$H/$^{29}$Si cross-polarization/magic-angle-spinning (CP/MAS) spectra were obtained on a Bruker AMX-400 spectrometer. The SP/MAS experiments were performed using a 45° pulse width with a relaxation delay of 2 min at a spinning rate of 7 kHz. The CP/MAS experiments were performed using a 6-ms contact time and a relaxation delay of 10 s. The spinning rates were 4 and 7 kHz for NaX-nano and NaX-$\mu$ samples, respectively.

Nitrogen isotherms at $T = 77$ K were determined using a volumetric adsorption apparatus (Micromerities, ASAP 2010). Before measurement, all samples were degassed at 200 °C until the pressure was less than 1 Pa and the degassing rate was less than 1 Pa min$^{-1}$. The surface area was estimated by the BET method, and the pore distribution was determined using a cylindrical pore geometry model (see below for details).

## Results and Discussion

Powder X-ray diffraction (XRD) patterns taken after different hydrothermal crystallization periods, while using the fumed silica source and maintaining the same temperature (60 °C) and shaking conditions (250 rpm), are presented in Figure 1. After the first day, only weak, broad zeolite "diffraction" peaks were observed (curve a). Both the intensity and sharpness of the diffraction peaks were significantly enhanced after a second day of crystallization (curve b), but they did not change appreciably after an additional 2 days of crystallization (curve c). These results indicate rapid formation of many zeolitic nuclei with very tiny grains at the beginning stages and relatively low crystal growth rates. It is likely that the synthetic conditions, relatively low crystalliza-

(17) Estermann, M.; McCusker, L. B.; Baerlocher, C.; Merrouche, A.; Kessler, H. *Nature* **1991**, *352*, 320.
(18) Zhan, B.-Z.; White, M. A.; Robertson, K. N.; Cameron, T. S. Gharghouri, M. *Chem. Commun.* **2001**, 1176.
(19) Kasahara, S.; Itabashi, K.; Igawa, K. In *Proceedings of the 7th International Conference on Zeolites*; Murakami, Y., Iijima, A., Ward, J. W., Eds.; Studies in Surface Science and Catalysis 28; Elsevier: New York, 1986; p 185.
(20) Zhan, B.-Z.; Li, X.-Y. *Chem. Commun.* **1998**, 349.
(21) Oriakhi, C. O. *J. Chem. Educ.* **2000**, *77*, 1138.

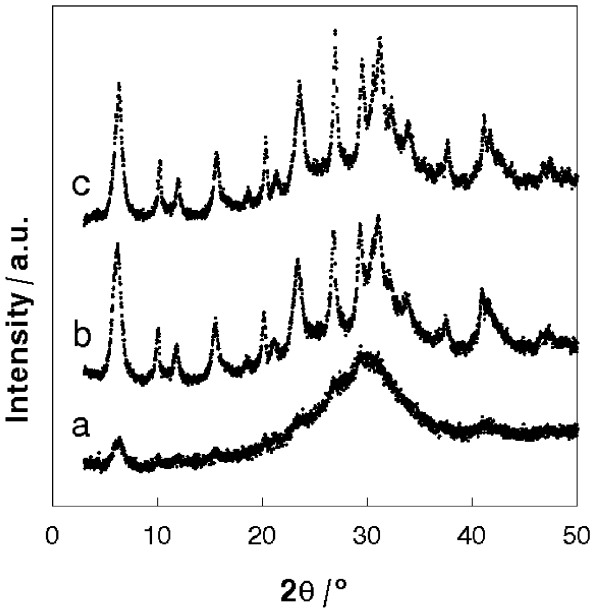


**Figure 1.** X-ray powder diffraction patterns after different crystallization times at 60 °C with shaking at 250 rpm for (a) 1, (b) 2, and (c) 4 days.

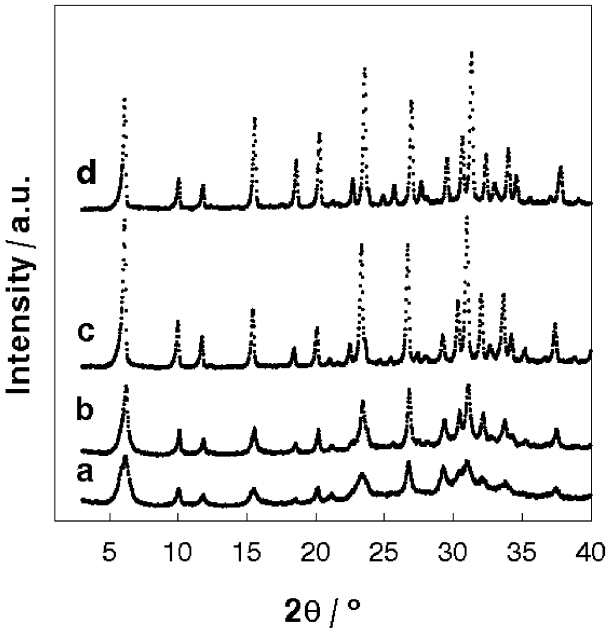


**Figure 2.** X-ray powder diffraction patterns for samples prepared using different synthetic conditions: (a) crystallization at 60 °C for 2 days with shaking, (b) crystallization at 45 °C for 2 days and then at 90 °C for 16 h with stirring, (c) crystallization at 90 °C for 2 days with no shaking, and (d) commercial sample NaX-Ald.

tion temperature and strong shaking, work together to accelerate nucleation efficiently while keeping the crystal growth rates low, thereby allowing production of ultrafine zeolitic crystals. All of the XRD patterns match very well with the simulated XRD powder pattern for FAU zeolite,[22] indicating that the synthesized crystals are pure FAU zeolite. From the diffraction peaks at $2\theta$ values of 6° [111], 16° [331], and 27° [642] and Scherrer's equation, we calculated[2,23] an average crystal dimension of $23 \pm 4$ nm for the sample crystallized at 60 °C for 4 days (NaX-nano).[18]

We have also found that crystallite sizes of NaX zeolites can be modified by changing the synthetic conditions. The XRD patterns in Figure 2 for samples produced using fumed silica under different crystallization conditions (different temperatures, shaking conditions, and crystallization times) clearly indicate that the diffraction peak widths and intensities of the as-synthesized samples greatly depend on the hydrothermal crystallization conditions. Crystallization at 90 °C for 2 days with no shaking or stirring gave the sharpest and most intense XRD peaks of the three methods presented (Figure 2c), indicating that much larger zeolite crystals were formed; the XRD pattern was comparable to that of the commercial sample NaX-Ald (Figure 2d), and from SEM (see below), the crystal sizes were found to be on the order of 1 $\mu$m (NaX-$\mu$). From other experiments, we have found that lowering the crystallization temperature or introducing agitation (stirring or shaking) during the crystallization period favors reduced particle sizes. Crystallization with shaking at 60 °C for 2 days gives NaX-nano (Figure 2a), whereas the sample crystallized in two stages (45 °C for 2 days followed by 90 °C for 16 h) with stirring gives an XRD pattern with peak widths and intensities between those of NaX-nano and NaX-$\mu$ (Figure 2b), and SEM results (see below) confirm the intermediate particle size for this sample. These results further demonstrate that nucleation processes and crystal growth rates, the key factors for the formation of particular particle size ranges of NaX, can be controlled by both crystallization temperature and shaking conditions.

An additional parameter that can influence the particle size of the product is the silicate source. This factor is important in the nucleation kinetics, as found recently for silica fibers.[24] Nanometer-sized silicate sources likely are a requirement for the formation of NaX-nano in our system. In addition to fumed silica, we have successfully achieved nanometer-sized NaX with both SM-30 silicate gel and TEOS sources. In the case of TEOS, we found that the hydration has to be conducted at 0 °C (ice−water bath) to obtain nanometer-sized aluminosilicate gel.

High-resolution scanning electron microscopy (HRSEM) images were recorded for the as-synthesized zeolitic samples, some of which are shown in Figure 3. Figure 3a clearly indicates that the particle size of NaX-nano is ultrafine and within a range of 20−100 nm, which is one of the smallest faujasite crystal sizes reported.[1,4,6] This size distribution is consistent with the results calculated from the XRD patterns, verifying that our method can indeed successfully synthesize ultrafine NaX crystals without the assistance of any organic templates. Figure 3b shows NaX-$\mu$ particles to be in the micron range (ca. 0.8 $\mu$m), again as expected from the XRD results. SEM results (Figure 3c) show that the particle size is about 300 nm for the sample judged to

(22) Treacy, M. M. J.; Higgins, J. B.; von Ballmoos, R. *Collection of Simulated XRD Powder Patterns for Zeolites*, 3rd ed.; Elsevier: New York, 1996.

(23) Cullity, B. D. *Elements of X-ray Diffraction*; Addison-Wesley: Reading, MA, 1978.

(24) Kleitz, F.; Marlow, F.; Stucky, G. D.; Schüth, F. *Chem. Mater.* **2001**, *13*, 3587.

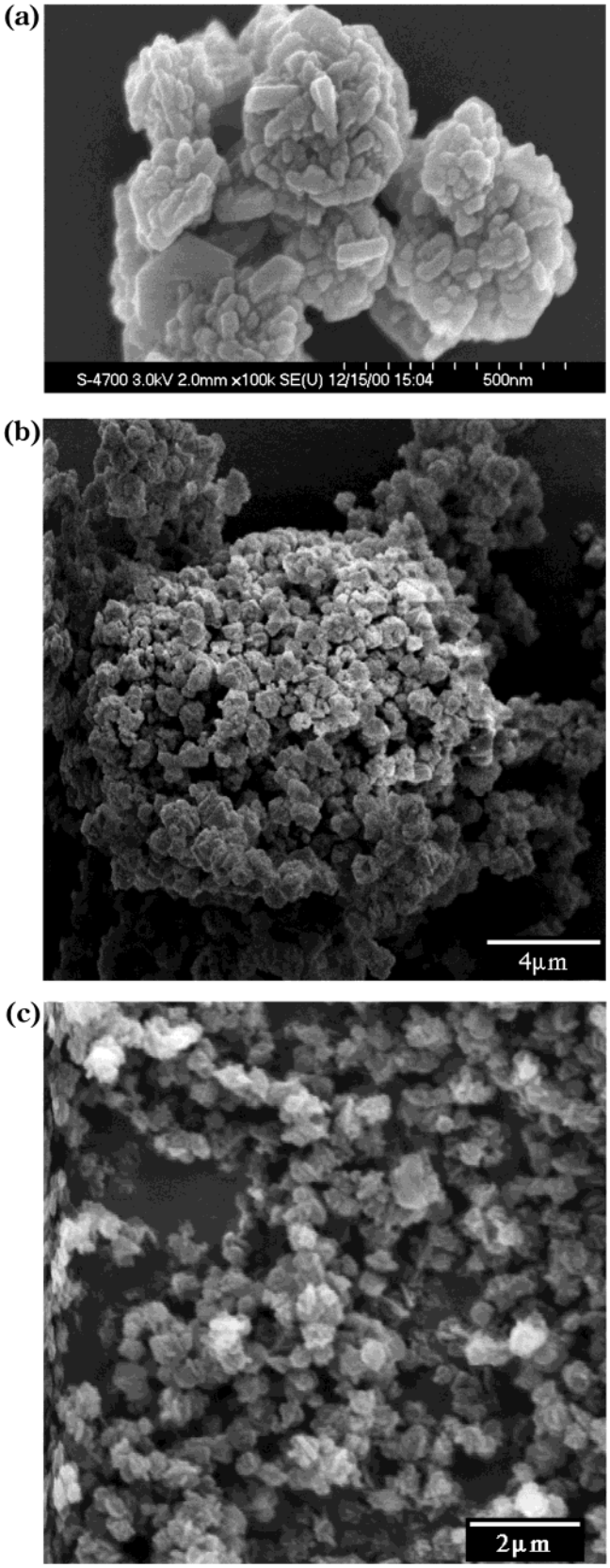


**Figure 3.** SEM images of (a) NaX-nano (uncoated) obtained on a Hitachi S4700 cold-field emission scanning electron microscope, (b) NaX-$\mu$ (gold-coated) obtained on a JEOL 35CF microscope using a 10-kV accelerating voltage; and (c) the intermediate-sized sample (gold-coated) for which the X-ray powder diffraction pattern is shown in Figure 2b, obtained on a JEOL 35CF microscope using a 10-kV accelerating voltage.

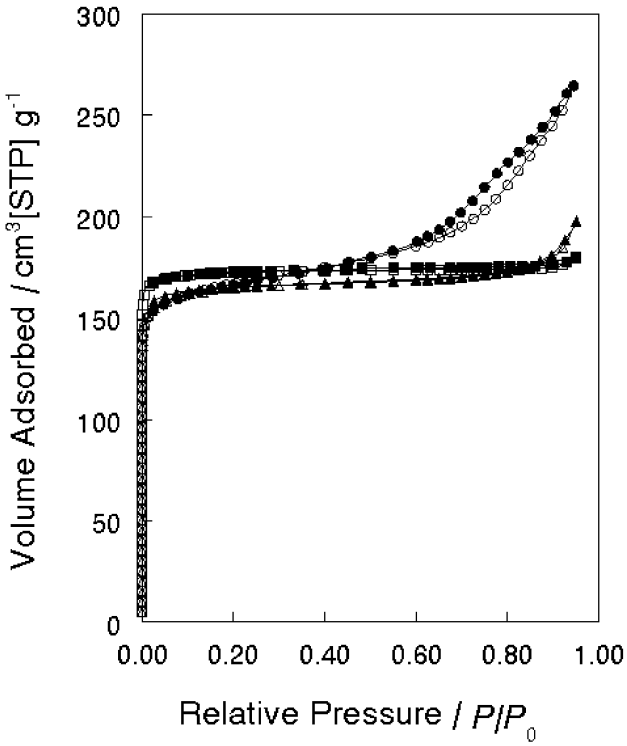


**Figure 4.** $N_2$ isotherms of NaX-nano (○, adsorption; ●, desorption), NaX-$\mu$ (△, adsorption; ▲, desorption) and NaX-Ald (□, adsorption; ■, desorption) at 77 K.

be intermediate between NaX-nano and NaX-$\mu$ (see Figure 2b for its XRD pattern). Judging from these results, we can easily tailor a variety of sizes of NaX zeolite, ranging from 20 nm to 1 $\mu$m, for various applications.

The $N_2$ adsorption isotherms of several different NaX samples are shown in Figure 4. NaX-$\mu$ gives a typical type I isotherm according to the classification of Brunauer et al.,[25] with complete filling of the micropore system at very low partial pressures. NaX-Ald behaves in a similar fashion. However, for NaX-nano, there is a hysteresis loop starting at $P/P_0 \approx 0.5$, indicative of a type III isotherm,[26] which can be explained by molecular nitrogen condensation in meso spaces. With NaX-nano, however, mesoporous space would only be formed from interparticle voids, because of the stacking of nanometer-sized crystalline particles. Porosity distributions for NaX-$\mu$, NaX-nano, and NaX-Ald were calculated from nonlocal density functional theory methods,[27] and these distributions are shown in Figure 5. All three samples exhibit a major peak at about 0.7 nm and then broad distributions of larger pores (5−30 nm), especially dominant in NaX-nano. From the *t*-plot analysis of the isotherms, carried out for $P/P_0 < 0.3$ as recommended,[28] the specific surface area and the external surface area were found to be $570 \pm 30$ and $43 \pm 5$ m$^2$/g, respectively, for NaX-$\mu$. The corresponding values were $530 \pm 30$ and $115 \pm 10$ m$^2$/g for NaX-nano. The increase in external surface is consistent with the reduction in particle size

(25) Brunauer, S.; Emmett, P. H.; Teller, E. J. *J. Am. Chem. Soc.* **1938**, *60*, 309.
(26) Kruk, M.; Jaroniec, M. *Chem. Mater.* **2001**, *13*, 3169.
(27) Olivier, J. P. *J. Porous Mater.* **1995**, *2*, 9.
(28) Rouquerol, F.; Avenir, D.; Faribridge, C. W.; Everett, D. H.; Haynes, J. H.; Pernicone, N.; Ramsay, J. D. F.; Sing, K. S. W.; Unger, K. K. *Pure Appl. Chem.* **1994**, *66*, 1739.

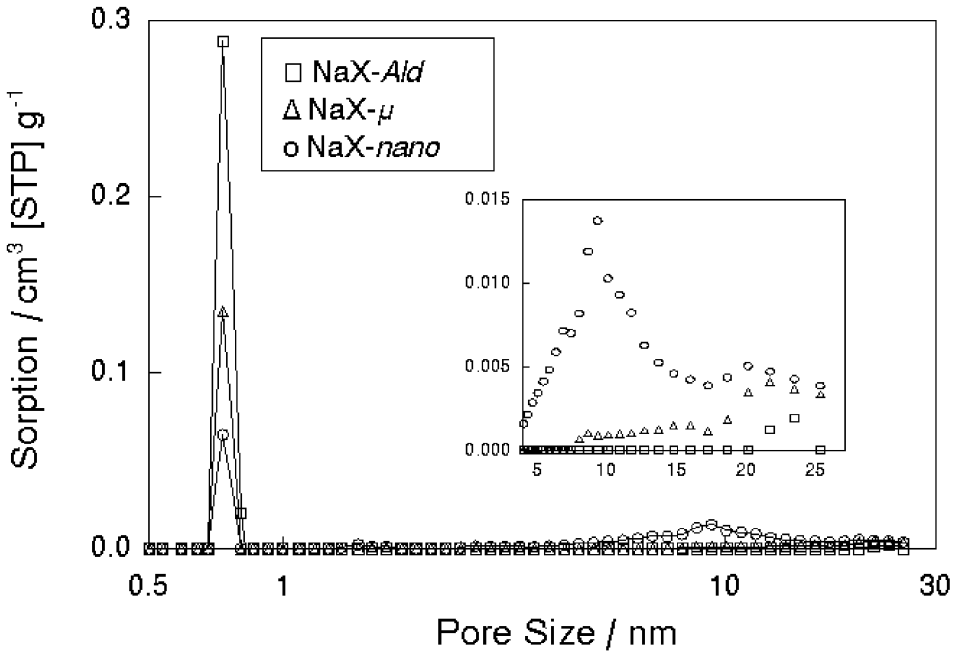


**Figure 5.** Porosities of NaX-nano, NaX-$\mu$, and NaX-Ald.

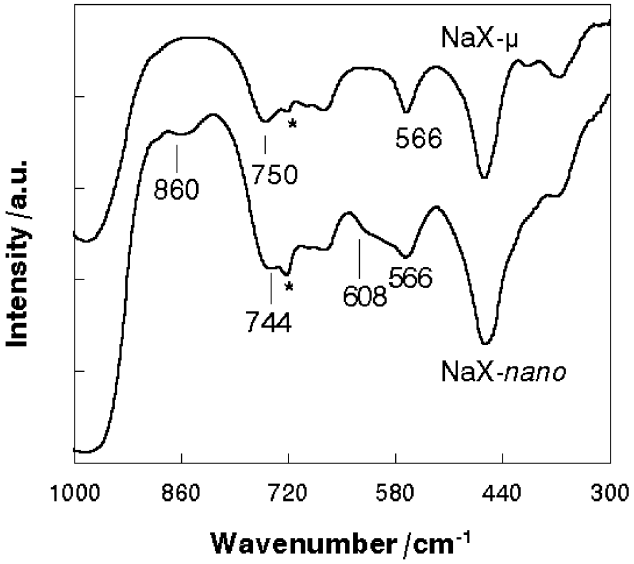


**Figure 6.** FT-IR spectra of NaX-nano and NaX-$\mu$. The peaks marked with * are attributed to Nujol.

observed by HRSEM. However, if the NaX-$\mu$ sample were composed of perfect 0.8 ± 0.2 $\mu$m cubes, its external surface would be expected to be 5 ± 1 m$^2$/g, much less than that observed, indicating that there is significant surface roughening of the NaX-$\mu$ sample, as observed in the SEM images (Figure 3). On the other hand, if the NaX-nano sample consisted of perfect cubes, each 23 ± 4 nm on all sides (this is the average particle size from the analysis of the X-ray powder diffraction data), this would lead to an external surface area of 180 ± 40 m$^2$/g, in fairly good agreement with 115 ± 10 m$^2$/g observed, indicating that the surfaces of NaX-nano are much smoother than those of NaX-$\mu$.

Both NaX-nano and NaX-$\mu$ were further characterized by FT-IR spectroscopy, as shown in Figure 6. Three features were noted. First, a symmetric stretching band at 744 cm$^{-1}$ was observed in NaX-nano,[29,30] with a corresponding peak at 750 cm$^{-1}$ in NaX-$\mu$. Second, the double-ring vibration at 566 cm$^{-1}$, characteristic of faujasite zeolites, appears as two bands at 608 and 566 cm$^{-1}$ in NaX-nano. Third, a new broad band at 860 cm$^{-1}$ was observed in NaX-nano, and it can reasonably be assigned to the silanol (Si−OH) bending mode associated with the $Q^3$ silicon species (Si connected to three O atoms that have connections to Si or Al),[30] detected with $^{29}$Si solid-state NMR spectroscopy, as discussed below. The existence of an abundance of silanol groups is attributed to the significant increase of the external surface area, demonstrated from the $N_2$ adsorption experiments.

High-resolution solid-state NMR techniques, such as magic angle spinning (MAS), are powerful structural tools in studying molecular sieve materials.[30−34] Micrometer-sized faujasite-X and -Y zeolites with 4-coordinate silicons (referred to as $Q^4$) in the frameworks have been intensively investigated with $^{29}$Si MAS NMR spectroscopy and the chemical shifts for the five $Q^4$ species Si(OAl)$_4$, Si(OAl)$_3$(OSi), Si(OAl)$_2$(OSi)$_2$, Si(OAl)(OSi)$_3$, and Si(OSi)$_4$ are assigned at approximately −84, −89, −94, −99, and −103 ppm, respectively.[30−34] Only a few reports have focused on silicon atoms linked to one hydroxyl group ($Q^3$) or two hydroxyl groups ($Q^2$) in faujasite zeolites.[35−38] Because of the presence of nearby protons, the $^1$H/$^{29}$Si cross-polarization/magic-angle-spin-

(29) Davis, J. E. D.; Förster, H. Vibrational Spectroscopy. In *Comprehensive Supramolecular Chemistry*, *Vol. 8: Physical Methods in Supramolecular Chemistry*; Davis, J. E. D., Ripmeester, J. A., Eds.; Elsevier Science Ltd.: Oxford, U.K., 1996; pp 33−119.
(30) Szostak, R. *Molecular Sieves: Principles of Synthesis and Identification*; Van Nostrand Reinhold: New York, 1989.
(31) Klinowski, J. *Chem. Rev.* **1991**, *91*, 1459
(32) Klinowski, J. *Anal. Chim. Acta* **1993**, *283*, 929.
(33) Fyfe, C. A.; Feng, Y.; Grondey, H.; Kokotailo, G. T.; Gies, H. *Chem. Rev.* **1991**, *91*, 1525.
(34) Fyfe, C. A.; Kokotailo, G. T. *NATO ASI Ser. C: Math. Phys. Sci.* **1994**, *447*, 277.
(35) Engelhardt, G.; Lohse, U.; Samoson, A.; Mägi, M.; Tarmak, M.; Lippmaa, E. *Zeolites* **1982**, *2*, 59.
(36) Grobet, P. J.; Jacobs, P. A.; Beyer, H. K. *Zeolites* **1986**, *6*, 47.
(37) Brunner, E. *J. Mol. Struc.* **1995**, *355*, 61.
(38) Rakiewicz, E. F.; Mueller, K. T.; Jarvie, T. P.; Sutovich, K. J.; Roberie, T. G.; Peters, A. W. *Microporous Mater.* **1996**, *7*, 81.

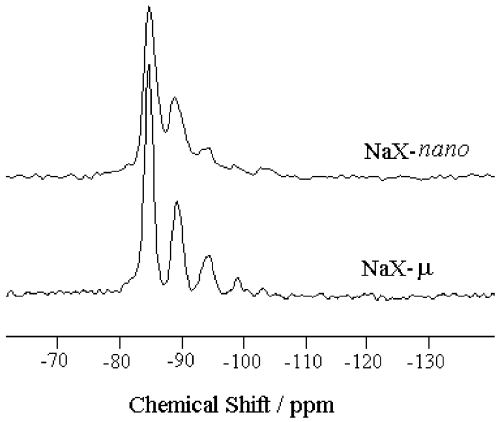


**Figure 7.** Solid-state single-pulse/magic-angle-spinning $^{29}$Si spectra of NaX-nano and NaX-$\mu$.

ning (CP/MAS) technique is adopted when studying $Q^3$ and $Q^2$ silicons, leading to sensitivity enhancements. However, quantification is still not easy for three reasons: (a) the efficiency of cross-polarization strongly depends on the distance between the silicon and the hydrogen atom, but the $Q^3$ atoms arising from dealumination or crystal defects are weak and random; (b) the presence of hydrogens belonging to organic templates might also be involved in cross-polarization; and (c) there is often overlap with $Q^4$ species. NaX-nano, prepared via the organic-additive-free approach, could provide ideal crystals to study the $Q^3$ species from the very large external surface (more than 20% of the total surface area, as determined from the $N_2$ adsorption studies). The $Q^3$ and $Q^2$ species arising from crystal defects likely are negligible in the NaX-nano sample, because there was no further thermal treatment. The presence of $Q^3$ species in the NaX-nano sample is also evidenced by the IR spectrum (Figure 6).

Single-pulse/magic-angle-spinning (SP/MAS) and CP/MAS techniques were used to measure $^{29}$Si NMR spectra for both NaX-nano and NaX-$\mu$ samples, primarily to determine the presence of $Q^3$ species in NaX-nano. The SP/MAS $^{29}$Si NMR spectra of both NaX-nano and NaX-$\mu$ are shown in Figure 7. The NaX-$\mu$ sample gives all five $^{29}$Si signals for $Q^4$ at −84.8, −89.5, −94.2, −99.3, and −103.1 ppm, which can be assigned to Si(OAl)$_4$, Si(OAl)$_3$(OSi), Si(OAl)$_2$(OSi)$_2$, Si(OAl)(OSi)$_3$, and Si(OSi)$_4$, respectively. Applying the formula

$$(\mathrm{Si/Al})_{\mathrm{NMR}} = \frac{I_4 + I_3 + I_2 + I_1 + I_0}{I_4 + 0.75I_3 + 0.5I_2 + 0.25I_1} \qquad (1)$$

where $I_n$ is the area of the NMR peak corresponding to the Si($n$Al) building unit, we calculate a Si/Al ratio of 1.2 for NaX-$\mu$, which is consistent with the result from the X-ray fluorescence analysis. NaX-nano also gives the five $Q^4$ peaks as for NaX-$\mu$. Furthermore, there are some shoulders broadening its SP/MAS NMR spectrum. These weak shoulders likely are due to the contribution of $Q^3$ species.

For NaX-$\mu$, there was no obvious difference between the SP/MAS and CP/MAS spectra as shown in Figure 8. This means that the contribution of the $Q^3$ species in NaX-$\mu$ is too small to be detected. However, the situation is quite different in NaX-nano: compared to the SP/MAS spectrum, the CP/MAS NMR spectrum (Figure 9)

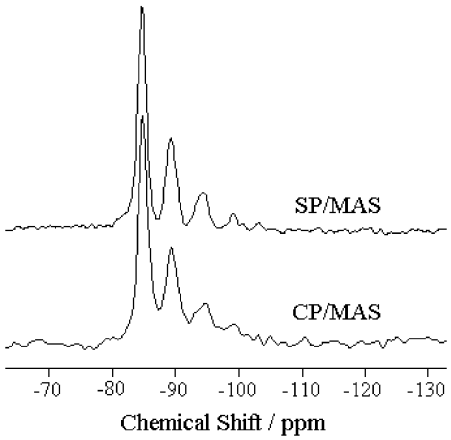


**Figure 8.** Solid-state single-pulse and $^1$H/$^{29}$Si cross-polarization/magic-angle-spinning spectra of NaX-$\mu$.

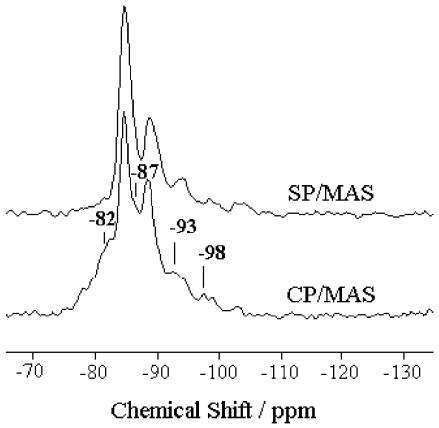


**Figure 9.** Solid-state single-pulse and $^1$H/$^{29}$Si cross-polarization/magic-angle-spinning spectra of NaX-nano. New/enhanced peaks are marked.

shows four enhanced/new peaks located at about −82, −87, −93, and −98 ppm, which can be reasonably assigned to silicon species linking to hydroxyl, i.e., $Q^3$.

In silicate-1, the $Q^3$ NMR shift of Si(OSi)$_3$(OH) was −103 ppm, about 9 ppm downfield with respect to Si(OSi)$_4$ at −112 ppm.[5] In a highly dealuminated faujasite zeolite, the Si(OSi)$_3$(OH) signal was observed at −100 ppm, about 7 ppm downfield relative to Si(OSi)$_4$ at −107 ppm.[37] In comparison with −103 ppm for Si(OSi)$_4$ observed in NaX-nano, we can reasonably assign the signal at −98 ppm to Si(OSi)$_3$(OH). It is well-known that the replacement of a silicon atom with an aluminum atom causes an approximate 5−6 ppm downfield shift in the $^{29}$Si NMR signals of zeolite materials. Therefore, the remaining three peaks at −93, −87, and −82 ppm can be assigned to the other three $Q^3$ species Si(OAl)(OSi)$_2$(OH), Si(OAl)$_2$(OSi)(OH), and Si(OAl)$_3$(OH), respectively. Among them, Si(OAl)$_2$(OSi)(OH) and Si(OAl)$_3$(OH) show greater intensity. To the best of our knowledge, this is the first time that all four $Q^3$ species have been observed in a faujasite zeolite.

## Conclusions

Various NaX zeolitic crystals with controlled sizes and surface properties have been synthesized with a newly developed organic-template-free approach using appropriate silicate sources and control of hydrothermal crystallization conditions, such as temperature and agitation. Ultrafine NaX zeolite (20−100 nm) was

prepared by growth at 60 °C for 4 days using silica, silica colloid, or TEOS as the silicate source. Several techniques, including $N_2$ adsorption and FT-IR and solid-state NMR spectroscopies, were employed to characterize all of the synthesized materials. Compared with the micrometer-sized NaX zeolite, the nanozeolite displays a huge external surface (about 20% of its specific surface area) and larger portion of 2−20-nm mesopores. Both FT-IR and $^{29}Si$ solid-state NMR spectra reveal an abundance of $Q^3$ silicon atoms (silanol groups) in NaX-nano.

**Acknowledgment.** We thank Neil Burford, Jeff Dahn, David Stevenson, and Robert White for help in this work. We are grateful to Hitachi, Mountainview, CA, for the use of the S-4700 SEM instrument. This research was financially supported by the Natural Sciences and Engineering Research Council and the Killam Trusts (the latter for a postdoctoral research fellowship to B.Z.Z. and research professorship to M.A.W.).

CM011635F